Biosensors and Bioelectronics 145 (2019) 111706

Contents lists available at ScienceDirect

Biosensors and Bioelectronics

journal homepage: www.elsevier.com/locate/bios

Fluorescent hydrogel test kit coordination with smartphone: Robust performance for on-site dimethoate analysis

Deshuai Kong[a], Rui Jin[a], Tianshuang Wang[a], Hongxia Li[a,b], Xu Yan[a,*], Dandan Su[a], Caileng Wang[a], Fangmeng Liu[a], Peng Sun[a], Xiaomin Liu[a], Yuan Gao[a], Jian Ma[a], Xishuang Liang[a], Geyu Lu[a,**]

[a] State Key Laboratory on Integrated Optoelectronics, College of Electronic Science and Engineering, Jilin University, Changchun, 130012, China
[b] Department of Food Quality and Safety, College of Food Science and Engineering, Jilin University, Changchun, 130062, China

ARTICLE INFO

Keywords:
Hydrogel
Portable kit
Smartphone
CuNPs
Dimethoate

ABSTRACT

Precise monitoring of pesticide with portable device was challenging because it required high sensitivity, short response time, strong stability and excellent selectivity. Herein, we newly constructed a stimuli-responsive hydrogel (SRHg)-based portable kit by embedding copper nanoparticles (CuNPs) in agarose hydrogel. In this work, dimethoate as inhibitor of urease restrained the generation of ammonia, which reduced in-situ etching of CuNPs, resulting in the fluorescence color response of test kit under ultraviolet illumination. Interestingly, by means of smartphone-based nanocolorimetry, the photo image of portable kit could be translated into digital information using ImageJ software, achieving a direct quantitative tool for dimethoate identification. The simplicity of SRHg-based portable kit combined with smartphone-based color recognition not only improved the analysis sensitivity (detection limit of 1.0 μg L^{-1}), accuracy and stability, but also simplified operation process and shortened sample-to-answer analysis time (55 min), demonstrating that the methodology met the needs of daily testing and provided a new sight for on-site monitoring of food safety and human health.

1. Introduction

Pesticides play an essential role for boosting agricultural production and guaranteeing food storage via controlling pests in agricultural activities (Pundir and Malik, 2019; Supraja et al., 2019; Vikrant et al., 2018). Dimethoate, as a typical representative of organophosphorus pesticides, have been widely employed for defending sucking insect infestation. However, pesticide contamination due to the extensive use and improper disposal of dimethoate has become one of the most tough public challenge in the pursue of sustainable agricultural development (Liu et al., 2019; Yan et al., 2018). In particular, dimethoate can work as a neurotoxin by inhibiting the activity of acetylcholinesterase (AChE) at the central nervous system, even in low concentration, causing cholinergic toxicity, which further damage to human health or even fatal consequences. For proper management of pesticide, accurate assessment of its pollution is a prime demand to protect human health and safeguard the food quality. Highly accurate quantitation of pesticide residuals in agro-products has been achieved using gold standard methods, such as gas chromatography, high-performance liquid chromatography and mass spectrometry (Masia et al., 2016; Parrilla Vázquez et al., 2019). Although these techniques possess forceful ability of trace analysis, the requirement of sophisticated instrumentation, time-consuming process and the lack of pocket-size device severely limit their on-site application, especially the real-time monitoring in emergency cases (Aragay et al., 2012; Arduini et al., 2019). In light of the limitations of the traditional strategies, there is significant motivation to investigating alternative approaches for detecting dimethoate in a speedy, facile and selective manner.

Owing to their cost-effectiveness, ultra-facile operation and portability, commercially available colloidal nanoparticles-based test strips for home and personal use to qualitative or semiquantitative screening of pesticide are based on the color change, which can be visually observed by naked eyes (Ge et al., 2014; Yan et al., 2017a). However, these on-site approaches cannot recognize the subtle change of target, making it unsuitable for tracing pesticide (Hakonen and Beves, 2018). Furthermore, paper-based strips are lack of stability (Mahato et al., 2017; Quesada-Gonzalez and Merkoci, 2015). To satisfy the needs of rapid, stable and accurate quantitative analysis, other solid sensing

* Corresponding author.
** Corresponding author.
E-mail address: yanx@jlu.edu.cn (X. Yan).

https://doi.org/10.1016/j.bios.2019.111706
Received 28 June 2019; Received in revised form 2 September 2019; Accepted 13 September 2019
Available online 18 September 2019
0956-5663/

phase carriers that provides easy and efficient recognition is highly desirable. Recently, taking advantage of mechanical stability and flexibility, stimuli-responsive hydrogels (SRHg) arouse increasing attention in sensing, actuators and biomedical fields (Caliari and Burdick, 2016; Hao et al., 2017; Li and Mooney, 2016; Willner, 2017). Not surprisingly, by recording the direct signal transitions upon application of external triggers, SRHg-based sensors possess fantasy perspectives in point-of-care (POC) testing fields with an effect to make analysis more accessible (Li et al., 2016; Yan et al., 2013; Zhan et al., 2019; Zhu et al., 2014). The hydrogel is arguably a favorable scaffold for detecting pesticide (Cui et al., 2019; Jin et al., 2019; Wu et al., 2019), however, it still remains hugely unexplored so far, especially for POC testing in food samples. Promoting the performance in on-site monitoring are achieved via the following approaches: strengthening the output signal and improving the stability (Cheng et al., 2018). In the first process, fluorescent nanomaterials as signal indicator can enhance the recognition due to their outstanding chemical and physical characteristics (Dong et al., 2017; Yan et al., 2019). In the other approach, fabricating a hydrogel-responsive device with mechanical stability is potentially effective (Hu et al., 2019; Zhang et al., 2018).

Inspired by the above-mentioned development, we herein designed copper nanoparticles (CuNPs)-rooted agarose hydrogel kit with stimuli-responsive characteristics for the accurate monitoring of dimethoate in a selective and sensitive manner (Scheme 1). CuNPs were first preloaded in the agarose hydrogel as signal indicator to manufacture the portable kit using a commercial 96-well microplate. In this sensing system, nonfluorescent CuNPs can be converted into green-emission fluorescent copper nanoclusters (CuNCs) by employing aqueous ammonia (NH_3)-triggered in situ etching process. The concentration of NH_3 was controlled by urease-catalyzed hydrolysis reaction of urea, accordingly, this proposed NH_3-controlled SRHg could be employed to detect the inhibitor of urease. In this portable platform, dimethoate as the target inhibit the activity of urease, further suppressed the hydrolysis reaction, accompanying the fluorescence (FL) signal change. For accurate quantification, the FL color variation of SRHg on the portable kit was recorded by the high-resolution camera of smartphone. Then the corresponding image could be translated into digital information based on ImageJ software, which shown linear relationship with the concentration of dimethoate. To be notable, by combing SRHg-based kit and smartphone reader, a skilled field operation platform was successfully applied to accurately detect dimethoate level in pear juice with acceptable results, making the analytical process convenience. Due to its great convenience and high stability, the availability of on-site portable kit made frequent screening and monitoring possible, providing a new way for guaranteeing the food safety and ensuring human health.

2. Experimental section

2.1. Materials and instruments

All commercially available reagents are purchased in analytical grade and used without further purification. Ascorbic acid (AA), urea, ammonium hydroxide ($NH_3{\cdot}H_2O$), Copper (II) nitrate trihydrate, sodium chloride, phenylalanine (PHE), prolin (Pro), tyrosine (Tyr), serine (Ser), valine (Val) and sodium hydroxide (NaOH) were got from Aladdin Reagent Co. Ltd (Shanghai, China). Urease was purchased from Sigma-Aldrich (Shanghai, China). AChE was obtained from Ryon Biological Technology Co., Ltd. (Shanghai, China). Metorlcard, Isoprocard, Paraoxonase, carbary, acetamiprid, Arprocard, nitenpyram, IMidaclothiz, thiacloprid and dimethoate were bought from Tianjin Zhongyi technology Co., Ltd. All reagents and solvents were analytical grade. All aqueous solutions were prepared using ultrapure water with resistivity higher than 18.2 MΩ cm. A UV-2550 spectrometer (Shimadzu) was used when need to know the UV–vis absorbance. The FL spectra were collected by using a RF-5301 PC spectrofluorophotometer (Shimadzu, Japan). The morphological structures were found by JEM- 7500 TEM (JEOL, Japan). X-ray photoelectron spectroscopy (XPS) was performed on an ESCALAB 250 XI electron spectrometer (Thermo).

2.2. Preparation of CuNPs

According to the method previously reported (Jia et al., 2013), the AA was used as a reducing-cum-capping agent for preparing CuNPs. Briefly, $Cu(NO_3)_2$ solution (100 mmol L^{-1}, 1.0 mL) add dropwise to the AA aqueous solution (100 mmol L^{-1}, 10 mL) under vigorous stirring. The reaction mixture was left to stir for 60 min at room temperature. Then, CuNPs were obtained.

2.3. Preparation of a pesticide detection kit for dimethoate

Portable detection kit was prepared: adding the agarose (10 mg mL^{-1}) to 100 °C boiling water, 900 μL of CuNPs solution and 225 μL of NaOH (30 mmol L^{-1}) were added into the hydrogel when cool the solution to 40 °C. After blending well, 150 μL of the prepared

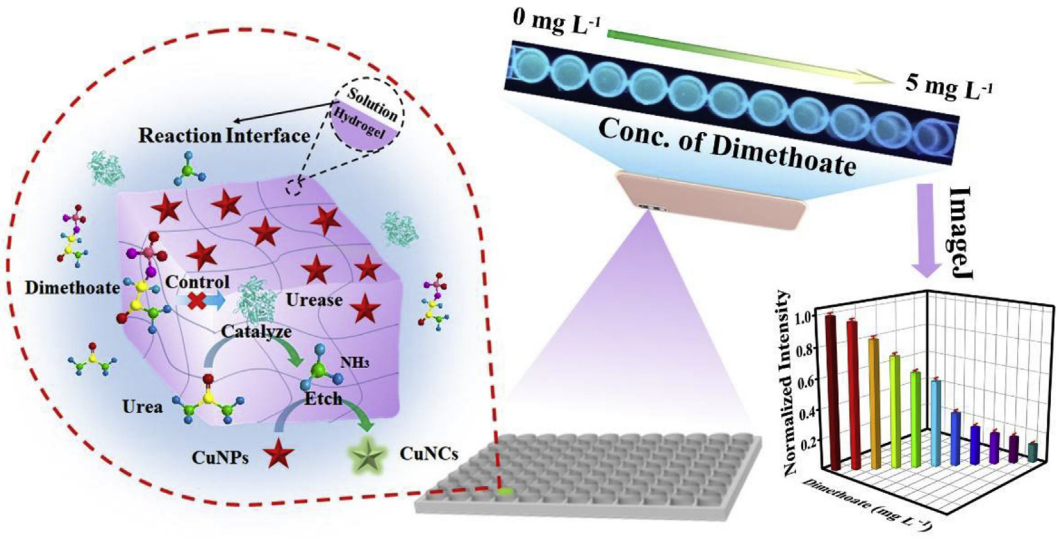

Scheme 1. Schematic illustration of SRHg-based portable kit for dimethoate assay.

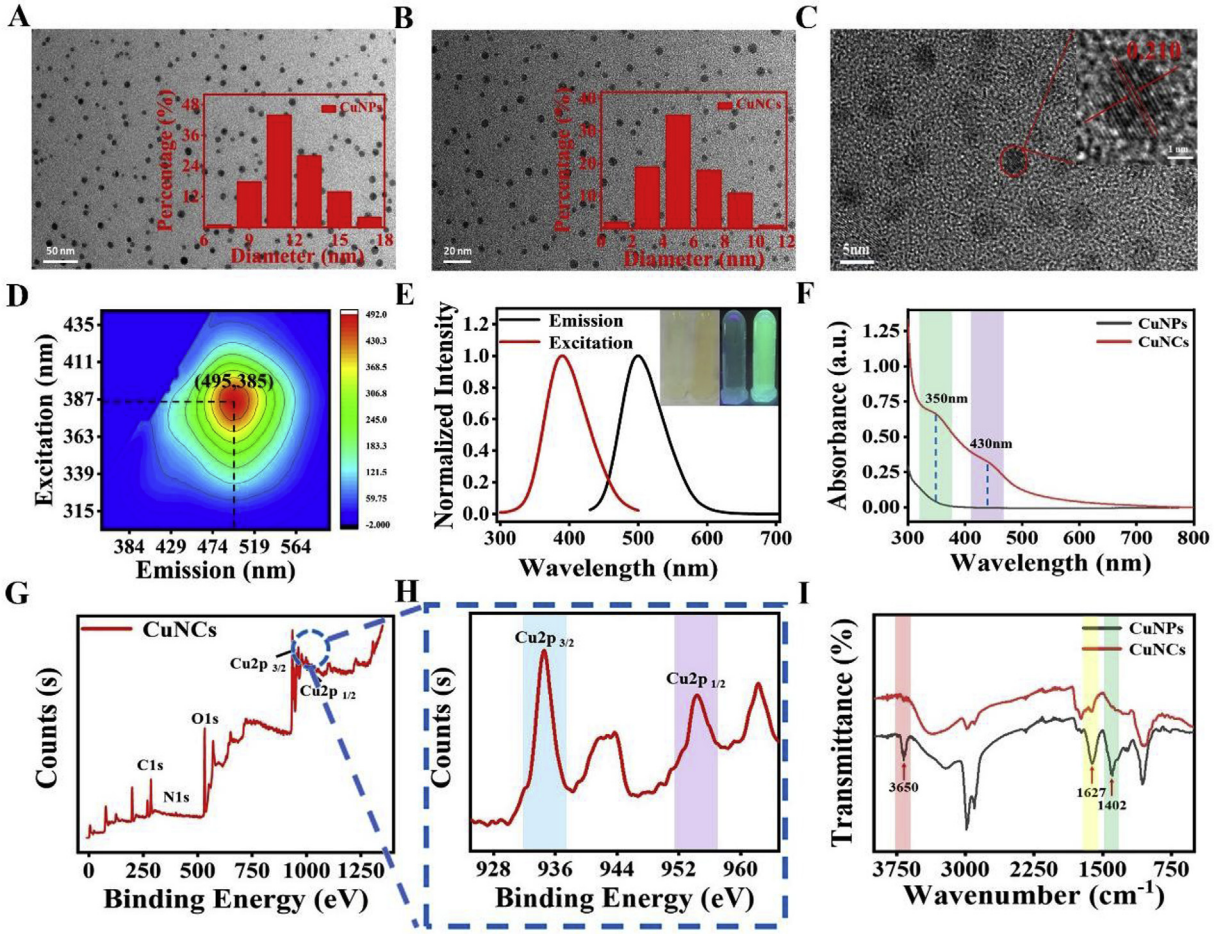

Figure 1. (A) TEM image of CuNPs, the illustration is size distribution of CuNPs. (B) TEM image of CuNCs, the illustration is size distribution of CuNCs. (C) HRTEM images of CuNCs at a scale of 5 nm. (D) Contour map of CuNCs sample obtained by fully synchronous fluorescence scanning spectrum measurement. (E) FL excitation and emission spectra of CuNCs. (F) UV–Vis absorption spectra of CuNCs (red) and CuNPs (black). (G) XPS of CuNCs. (H) Amplified XPS of Cu 2p electrons. (I) FT-IR spectra of CuNPs (black) and CuNCs (red).

agarose was added to the 96-well microplate. The kit could be stored in room temperature for further use.

25 μL of dimethoate and 50 μL of urease (10 U mL^{-1}) were mixed for 30 min, then 125 μL of urea (10 mmol L^{-1}) was introduced to above mixture for 15 min. Finally, the reaction solution was added into kit well for incubating 10 min. Under ultraviolet light, the color of the hydrogel was recorded by smartphone and analyzed by ImageJ software.

3. Results and discussion

3.1. NH_3-triggered etching of CuNPs

Inspired by the reduction process (Deng et al., 2018), the CuNPs were facilely synthesized by introducing AA as reducing agent and capping reagent into Cu (II) solution for stirring 60 min at room temperature. As the transmission electron microscopy (TEM) image shown, the synthesized AA-stabilized CuNPs with good uniformity and the average diameter in size were 10.3 ± 1.8 nm (Fig. 1A). Through the size-focusing etching process of NH_3, the large-size CuNPs decomposed into CuNCs, whose status were highly monodispersed with average diameters of 4.9 ± 1.2 nm (Fig. 1B). The high-resolution TEM images in Fig. 1C showed that the lattice fringes of CuNCs (0.210 nm) were fit to that of metallic Cu, corresponding to the (111) lattice planes of Cu (Miao et al., 2015). These observations implied that NH_3 could successfully trigger the etching process of CuNPs. To gain insight into the FL mechanism of CuNCs, a series of characterization strategies had been successively carried out. Fig. 1D displayed the FL property of CuNCs, whose maximum emissions was 495 nm with the excitation wavelength changing from 310 nm to 440 nm, indicating that the emission wavelength of CuNCs exhibited independent-excitation feature. From the corresponding excitation-emission matrix of Fig. 1D, the photoexcitation and photoemission spectra were taken to show the symmetrically spectral peak (Fig. 1E), indicating the relatively uniform surface states in the proposed CuNCs. Inset showed the corresponding color of CuNPs and CuNCs under sunlight and ultraviolet lamp, revealing the etching of CuNPs. Subsequently, absorption spectra of CuNPs and CuNCs were depict in Fig. 1F. Compared with CuNPs, CuNCs newly exhibit two absorption band at 350 nm and 430 nm, which could be attributed to n-π* transition of C═O in AA-capped CuNCs. The X-ray photoelectron spectroscopy (XPS) survey spectrum revealed the presence of C, N, O and Cu in CuNCs (Fig. 1G). The Cu 2p spectrum exhibited two characteristic peaks at 934 eV and 954 eV, which were corresponding to Cu 2p1/2 and Cu 2p3/2, respectively, indicating that CuNCs were composed of Cu (0) (Fig. 1H) (Hu et al., 2018). Fourier transform infrared spectroscopy (FTIR) spectra were further used to explore the change of surface groups of nanomaterials. As revealed in Fig. 1I, disappearance of the characteristic absorption of O–H at 3650 cm^{-1} and 1402 cm^{-1} suggested that –OH of AA were oxidized in the presence of NH_3. Meanwhile, the C═C stretching vibration at 1627 cm^{-1} was red-shift after introducing NH_3, indicating that NH_3-trigged etching might be influence the surface groups of CuNPs.

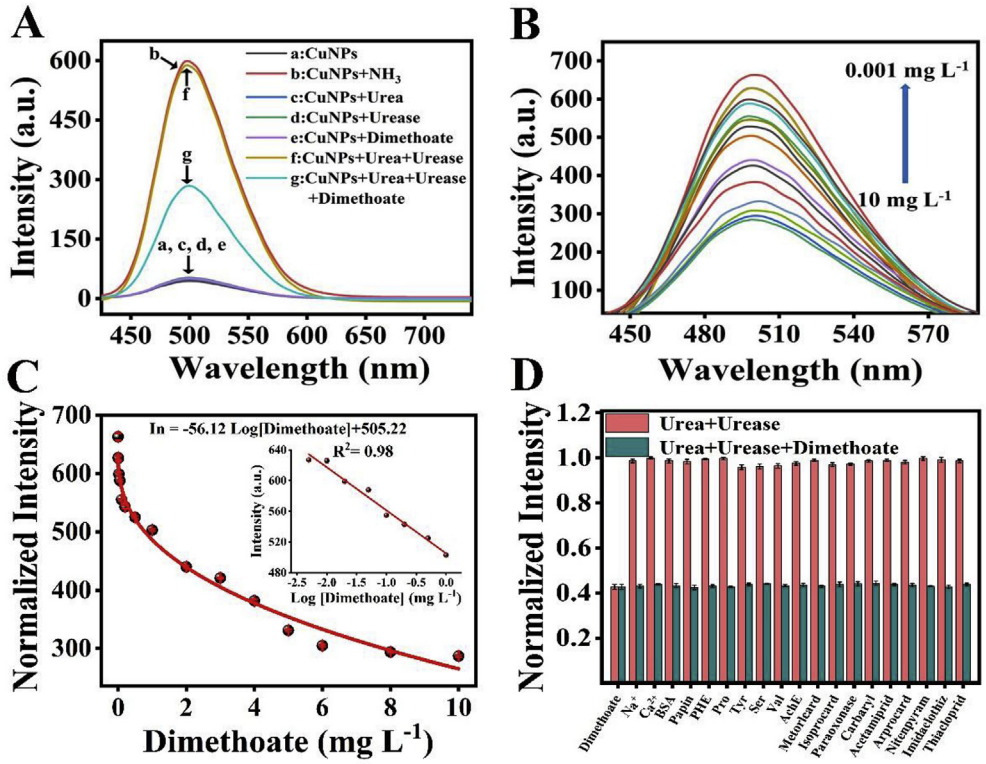

Fig. 2. (A) FL intensity of reaction solutions: CuNPs (a), CuNPs + NH_3 (b), CuNPs + Urea (c), CuNPs + Urease (d), CuNPs + Dimethoate (e), CuNPs + Urea + Urease (f), and CuNPs + Urea + Urease + Dimethoate (g). (B) FL intensity of system toward different concentration of dimethoate. (C) The trends of FL intensity with different concentration of dimethoate. Inset illustrated the relationship between logarithmic of dimethoate concentration and FL intensity. (D) FL intensity of system in the presence of interfering substances.

Owing to NH_3-induced etching reaction, CuNPs can be rapidly converted to CuNCs, which possessed bright FL emission. As showed in Fig. 2A, there were no obvious FL peaks in the presence of CuNPs (a line). When mixing the NH_3 and CuNPs, characteristic peak at 495 nm were appeared because of the formation of CuNCs (b line). It should be mentioned that weakly alkaline condition (3.0 mmol L^{-1} of sodium hydroxide) could greatly enhance the etching efficiency (Fig. S1A), further improving the sensitivity toward NH_3. In order to elucidate the performance of CuNPs, different amounts of NH_3 from 0.08 mmol L^{-1} to 6.67 mmol L^{-1} were added into solution, FL intensity gradually increased (Fig. S1B), obviously leading to a 5-fold intensity enhancement. Meanwhile, Fig. S1C displayed a clear relationship between FL intensity and the concentration of NH_3. In view of NH_3-triggered etching process, CuNPs could be employed as an optical indicator for sensing of NH_3-generated biocatalytic enzyme and its inhibitor.

3.2. Performance of probe

Bestowed with the sensitivity of NH_3-triggered etching of CuNPs, the system was employed to detect pesticide. Urease could specifically catalyze the degradation of urea to produce CO_2 and NH_3 (Beminger et al., 2018; Lei et al., 2016; Santopolo et al., 2019), controlling the etching of CuNPs (f line, Fig. 2A). Dimethoate as an inhibitor could block the activity of urease, preventing the formation of NH_3, which in turn caused the FL change of system (g line). To validate the sensing feasibility, urea, urease and dimethoate (c-e line) were separately introduced into CuNPs solution. There were no obvious FL signals in the systems, indicating that CuNPs could not be etched by those substances. The above experiments implied that CuNPs-based platform could be employed for profiling of dimethoate. In this sensing platform, urease was employed as antennae for catalytic hydrolysis toward urea and selective recognition to dimethoate. Thus, we systematically investigated the response of system toward urease. Under optimal conditions (Fig. S2), the FL intensity at 495 nm was gradually enhanced with increasing concentration of urease from 0.002 U mL^{-1} to 4.0 U mL^{-1} (Fig. S3). Meanwhile, Fig. S3C illustrated a good linear relationship between the concentration of urease and the FL intensities (R^2 = 0.99).

Owing to the good performance toward urease, the assay of pesticide detection was performed by employing CuNPs/Urease/Urea system. As expected, with the concentration of dimethoate increased from 0.001 to 10 mg L^{-1}, the FL intensity of system was gradually decreased which attributed to the inhibition of enzyme (Fig. 2B). The FL intensity change of system displayed a well linear fitting (R^2 = 0.98) with the logarithm of concentration of dimethoate (0.005–1.0 mg L^{-1}) in Fig. 2C. The regression equation was Intensity = −56.2 log [dimethoate] + 505.22, mg L^{-1}. It was worth mentioning that the detection limit (LOD) was calculated to be 0.002 mg L^{-1} (S/N = 3), which was lower than the value (0.05–1.0 mg L^{-1}) of maximum residue limit stipulated by Ministry of Agriculture of the people's Republic of China (GB-2763-2016), meeting the practice requirement. Compared with traditional quenching/recovery-based approaches, this detection strategy was based on the analyte-controlled formation of fluorophore, which offered a low background signal and overcame the poor stability of NCs (Qing et al., 2016; Tan et al., 2017). From a practical point of view, the selectivity had been investigated by introducing the common coexistence substances in agricultural and biological samples, such as Na^+, Ca^{2+}, bovine serum albumin (BSA), acetylcholine esterase (AChE), phenylalanine (PHE), proline (Pro), tyrosine (Tyr), serine (Ser), Valine (Val), metorlcard, isoprocard, paraoxon, carbaryl, acetamirid, arprocard, nitenpyram and thiacloprid. As depicted in Fig. 2D, after the addition of dimethoate, the FL intensity of CuNPs/Urease/Urea system was significantly decreased, while the FL intensity did not change in the presence of the above substances, proving that the sensing system exhibited a high selectivity toward dimethoate. Furthermore, other organophosphorus pesticides (OPs) and carbamate pesticide were also chosen to investigate the selectivity. Fig. S4 showed the normalized intensity of probe toward OPs and carbamate pesticide at concentration of 1.0 mg L^{-1}. Compared with AChE-based strategies (Chang et al., 2016; Long et al., 2015; Wang et al., 2016; Zhang et al., 2016), the CuNPs/Urease/Urea system possessed excellent selectivity toward dimethoate, which could distinguish dimethoate from other OPs. Taken

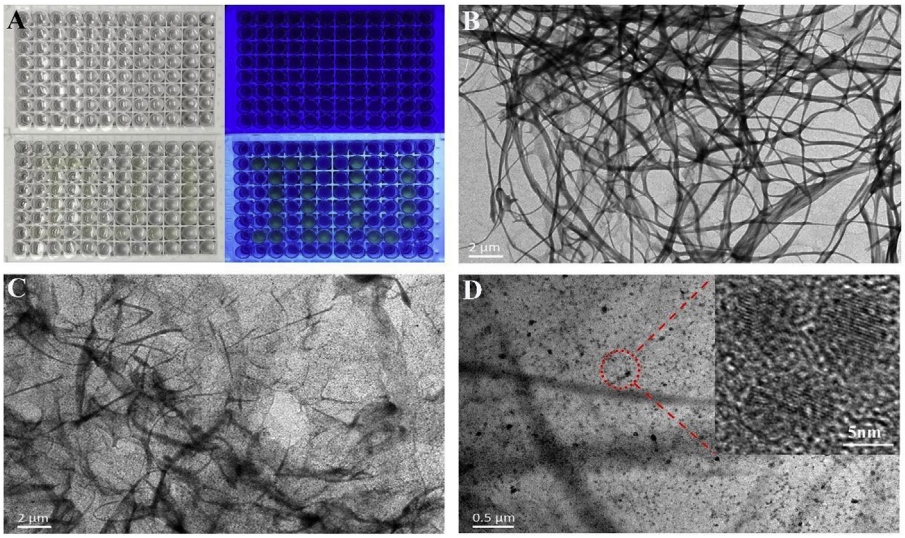

Fig. 3. (A) Photos of 96-well portable kit under sunlight and ultraviolet light. (B) TEM image of agarose hydrogel without CuNPs. (C) and (D) TEM images of CuNPs-loaded hydrogel under different magnifications.

together, the established system exhibited good sensitivity and high specificity, proving that the biosensor was suitable for dimethoate detection.

3.3. Precise sensing of dimethoate by a portable test kit

There is an urgent need for portable device that can on-site screening of pesticide in security and environmental applications for monitoring environmental pollution, safeguarding the food resources and estimating clinical poisoning (Kim et al., 2018). With above findings of FL response and proofs, we designed here a portable test kit by immobilizing CuNPs into agarose hydrogel to fabricate NH_3-controlled SRHg that could serve as a sensing platform for fluorometric detection of dimethoate. Thanks to its mechanical stability and flexibility, agarose-based SRHg with cross-linked 3D macromolecular networks as a robust supporter that undergo response to physicochemical stimuli possessed great perspectives in POC testing field (Bay et al., 2019; Hsu et al., 2019; Zhao et al., 2019). In this case, we manufacture CuNPs-rooted agarose hydrogel to 96-arrays using the commercial microplate without the need of potentially toxic cross-linking agents (Fig. 3A). To further understand the structural information, TEM tests were performed on agarose hydrogels containing CuNPs after vacuum freeze drying at low temperature. As depicted in Fig. 3B, TEM images clearly revealed the formation of porous layered structures of hydrogels, which could load abundant components. After introducing CuNPs, it could be easily observed that CuNPs were uniformly dispersed in highly branched frameworks of hydrogels (Fig. 3C). At high magnification (Fig. 3D), the branch of CuNPs-based hydrogel exhibited black spots that were identified as CuNPs based on the size (10 nm). As displayed in Fig. 3A, the as-fabricated portable kit showed no color under daylight and UV illumination. After writing "JLU" with NH_3 as ink to trigger etching, the kit immediately displayed with green color under UV light. The stability was a main characteristic of POC devices to estimate the performance of platform in practical applications. As revealed in Fig. S5, the portable kit achieved little FL color change for 14 consecutive hours, indicating that the kit could hold a relatively stable state for a certain period of time.

The sensing property of portable kit were firstly investigated by introducing NH_3 and urease (Fig. S6). For precise sensing of pesticide, various amounts of dimethoate (25 μL) were used to inhibit the activity of urease (50 μL, 10 U mL^{-1}) for 30 min. Then, urea (125 μL, 10 mmol L^{-1}) was introduced to produce NH_3. After reacting 15 min, the above solution was dropped into SRHg-based kit for another 10 min (Fig. 4A). To recognize the FL color response of SRHg, corresponding images of kit were recorded by smartphone (HUAWEI Nova 3e) built-in cameras (Fig. S7). As revealed in Fig. 4B, the color was changed in a distinct gradient, which offered a visual detection limit of 0.1 mg L^{-1} by independent observers. Through ImageJ software, converts optical image information to tonal parameters, which realized quantitative detection of dimethoate. Hue histogram showed in Fig. 4C can be considered as digital information that represented to the color-change detection. Through the image-processing method, a good linear relationship ($R^2 = 0.97$) between normalized hue intensity and the logarithm of concentration of dimethoate in the range from 0.001 mg L^{-1} to 5 mg L^{-1} was obtained from the test kit (Fig. 4D). These results proved that the integration of SRHg-based kit with smartphone afforded a portable strategy for precise monitoring of dimethoate. Furthermore, a comparison with other strategies for dimethoate detection were summarized in Table S1. The results illustrated that the proposed kit possessed good performance in term of linear range and detection limit. More interestingly, the detection time (sample-to-answer time 55 min) was comparable to or shorter than previous portable device, such as nanomaterials-based test strips (Wu et al., 2017; Yan et al., 2017b), glucose meters-based pocket-size device (Tang et al., 2019), and double-film screening card (Sun et al., 2017). Since we confirmed SRHg-based kit based on the in-situ chemical etching process, the test stability of kit was further investigated by incubating dimethoate to evaluate the performance. As display in Fig. S8, the kit achieved similar FL color change toward 5.0 mg L^{-1} of dimethoate within 14 h, implying that the kit maintained stable enough for sensing pesticide. Such excellent sensing performance might arise from the following distinctive features: (1) CuNPs as signal indicator not only offered a low background signal, but also overcame the poor stability of NCs, further improving the sensitivity of assay. (2) The SRHg-based kit that load abundant CuNPs showed greatly improved stability, making the operation facile for real-time detection. Compared with previous SRHg sensors that undergo structural changes (swelling or collapse), our proposed kit that relied on the FL color change of nanomaterials was more convenience and easy-to-use.

Selective identification of pesticide is key feature to estimate the practicality, especially in the POC testing. Therefore, to simulate the practical environment, the selectivity had been investigated by introducing common substances such as metal ion, protein, amino acid and pesticide. Fig. 4E depicted the FL color change upon above control

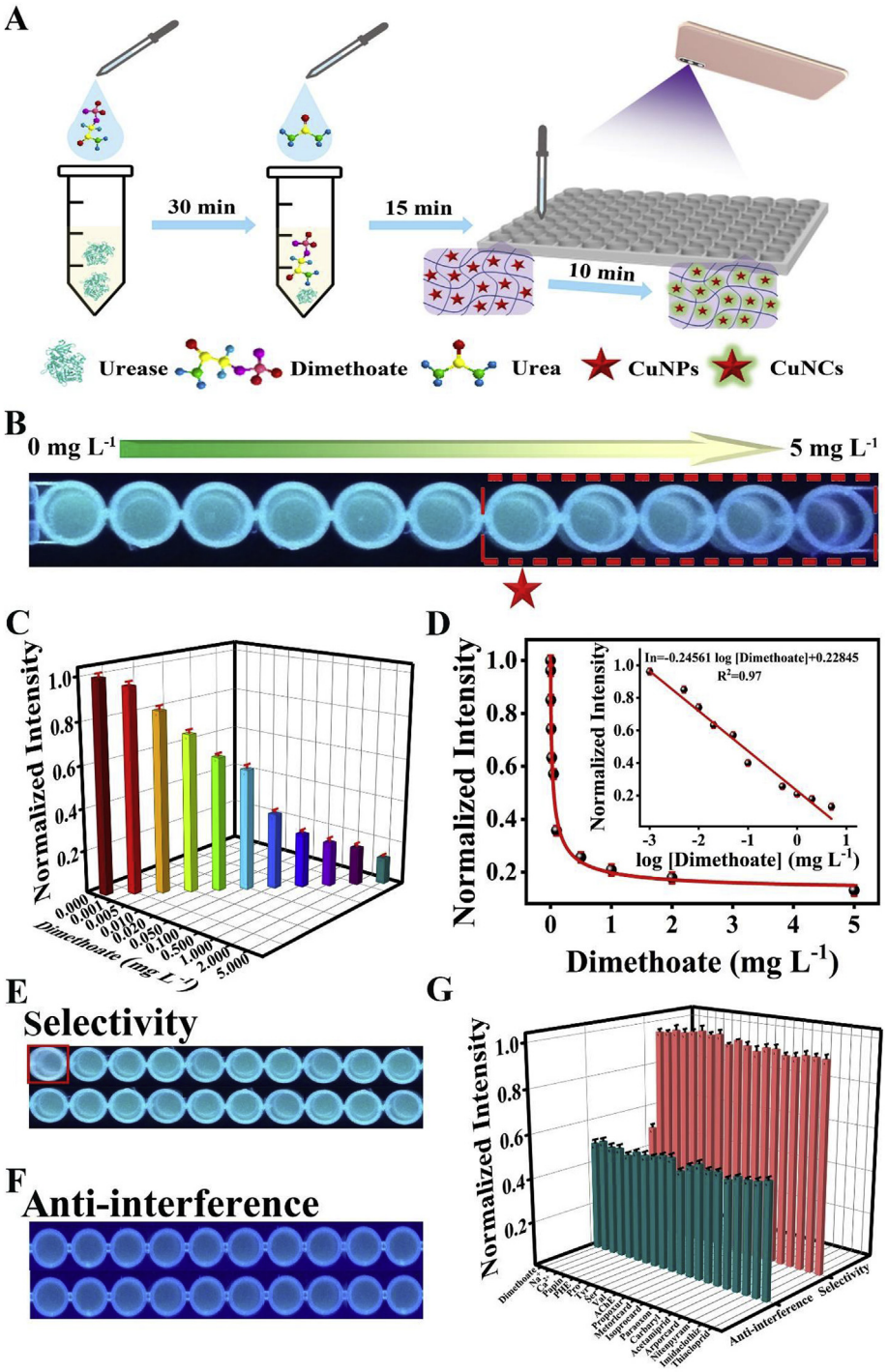

Fig. 4. (A) Reaction process of test kit. (B) The photograph of kit with different concentrations of dimethoate under UV lamp. (C) The normalized hue intensity digitized by ImageJ software. (D) Corresponding relationship between the concentration of dimethoate and hue intensity. (E) and (F) The corresponding photograph in the presence of interfering ions. (G) The selectivity and interference effect of kit.

interference substances. The normalized intensity histogram in Fig. 4F illustrated that the interference substances cannot trigger the inhibition of urease, generating negative FL signal. While only dimethoate ($1.0\,mg\,L^{-1}$) caused remarkable response. The excellent specificity of SRHg-based kit might due to enzyme-assisted specific recognition and NH_3-triggered CuNPs etching. Following, the anti-interference capacity of the SRHg-based kit was carried out via incubating the dimethoate and co-existing substances. As shown in Fig. 4G, the response of the SRHg-based kit toward dimethoate maintained constant in the presence of common interferences, revealing strong anti-interference capacity of kit. Thus, the solid CuNPs-based SRHg exhibited good strong anti-interference ability and specificity, proving that the portable kit was suitable for dimethoate detection.

3.4. Detection of dimethoate in pear sample

From the practical application of view, screening of pesticide in real samples is of a great significance. Pear juice was chosen as model matrix for investigating the on-site application. As illustrated in Fig. 5A, apparent FL color change of portable kit was dose-dependent in pear

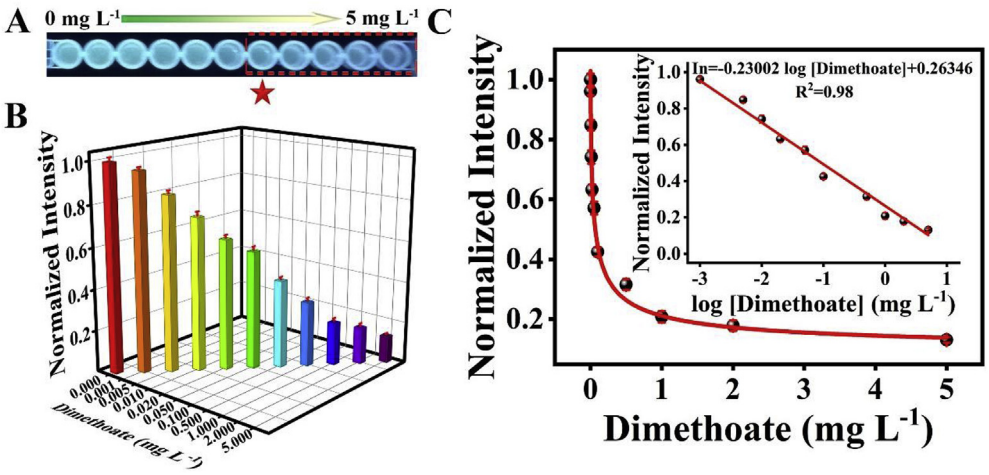

Fig. 5. (A) Different concentrations of dimethoate in pear juice using portable kit. (B) The hue intensity digitized by ImageJ software. (C) The change trend of hue intensity with the increase of dimethoate quantity.

Table 1
Determination results of dimethoate in pear juice samples.

Sample	Added (mg L^{-1})	Found (mg L^{-1})	Recovery (n = 3, %)	RSD (n = 3, %)
Pear juice	0.001	0.001	99.99	8.45
	0.05	0.051	101.03	1.02
	2.0	2.205	110.27	2.42

juice after introducing dimethoate in the range of 0.001–5.0 mg L^{-1}, which could be observed by naked eyes under the UV light (λ = 365 nm). The primary color of photo was converted into hue intensity and then digitized by ImageJ software (Fig. 5B) (Kong et al., 2019). The normalized hue intensity of SRHg-based portable kit possessed a good linear (R^2 = 0.98) fitting with the concentration of dimethoate via employing the image processing algorithm (Fig. 5C). It should be noting that the linear range of portable kit in pear juice sample was consistent with that of in double distilled water, demonstrating that pear matrix (dilution of 5-fold) possessed barely influence on the performance of kit. Following, the accuracy of POC kit in practice application was investigated by measuring the recovery of standard addition method. As presented in Table 1, the recoveries value ranged from 99.9% to 110.3%, which satisfied the monitoring requirements. Evidently, with rational designs, SRHg-based portable kit was suitable for POC testing of dimethoate with favorable sensitivity, accuracy and stability, offering outstanding protocol to protect human health and ensure food safety.

4. Conclusions

In summary, SRHg-based portable kit combined with smartphone-based nanocolorimetry was employed for on-site detection of dimethoate in a speedy, sensitive, selective and accurate manner. The designed test kit comprised CuNPs probe as signal indicator to recognize target and agarose hydrogel as solid phase scaffold to carry nanomaterials. This SRHg-based portable device could successfully accurate profiling of dimethoate based on the analyte-triggered transformation of nanomaterials, which not only offered a low background signal, but also overcame poor stability of CuNCs. Furthermore, compared with previous hydrogel-based sensor that undergo structural changes (swelling or collapse), our proposed SRHg that relied on the FL color change of nanomaterials was more convenience and suitable for POC testing. Particularly, by means of smartphone-based nanocolorimetry, the photo images of kit could be translated into digital information, achieving the on-site monitoring of dimethoate. Interestingly, the SRHg-based portable platform was employed for practical application with satisfactory recovery in pear samples. Owing to the merits of the remarkable stability and facile usage of SRHg, the high efficiency and good operability of the test kit showed great potential to quantitative POC testing of dimethoate for routine monitoring pollution and estimating poisoning.

Author agreement

We the undersigned declare that this manuscript is original, has not been published before and is not currently being considered for publication elsewhere. We confirm that the manuscript has been read and approved by all named authors and that there are no other persons who satisfied the criteria for authorship but are not listed. We further confirm that the order of authors listed in the manuscript has been approved by all of us. We understand that the Corresponding Author is the sole contact for the Editorial process. He is responsible for communicating with the other authors about progress, submissions of revisions and final approval of proofs.

CRediT authorship contribution statement

Deshuai Kong: Conceptualization, Data curation, Methodology, Writing - original draft. **Rui Jin:** Writing - original draft, Methodology. **Tianshuang Wang:** Methodology. **Hongxia Li:** Validation, Data curation, Funding acquisition. **Xu Yan:** Methodology, Writing - original draft, Conceptualization, Supervision, Funding acquisition. **Dandan Su:** Data curation. **Caileng Wang:** Methodology. **Fangmeng Liu:** Methodology. **Xiaomin Liu:** Writing - review & editing. **Yuan Gao:** Validation. **Jian Ma:** Validation. **Xishuang Liang:** Writing - review & editing. **Geyu Lu:** Funding acquisition, Supervision, Writing - review & editing, Funding acquisition, Methodology.

Declaration of competing interest

The authors declare that they have no known competing financial interests or personal relationships that could have appeared to influence the work reported in this paper.

Acknowledgements

This work was supported by the National Key Research and Development Program of China (No. 2016YFC0207300). Program for JLU Science and Technology Innovative Research Team (No. JLUSTIRT 2017TD-07). The National Nature Science Foundation of China (No. 21806051, 31901777, 61831011, 61722305 and 61833006). Science and Technology Development Program of Jilin Province (No. 2017052016JH). Scientific and Technological "13th Five-Year Plan" Project of Jilin Provincial Department of Education (No. JJKH20190111KJ). The Graduate Interdisciplinary Research Fund of Jilin University (No. 10183201833). The Graduate Innovation Fund of Jilin University (No. 101832018C016).

Appendix A. Supplementary data

Supplementary data to this article can be found online at https://doi.org/10.1016/j.bios.2019.111706.

References

Aragay, G., Pino, F., Merkoci, A., 2012. Chem. Rev. 112, 5317–5338.
Arduini, F., Cinti, S., Caratelli, V., Amendola, L., Palleschi, G., Moscone, D., 2019. Biosens. Bioelectron. 126, 346–354.
Bay, H.H., Vo, R., Dai, X.C., Hsu, H.H., Mo, Z.M., Cao, S.R., Li, W.Y., Omenetto, F.G., Jiang, X.C., 2019. Nano Lett. 19, 2620–2626.
Beminger, T., Bliem, C., Piccinini, E., Azzaroni, O., Knoll, W., 2018. Biosens. Bioelectron. 115, 104–110.
Caliari, S.R., Burdick, J.A., 2016. Nat. Methods 13, 405–414.
Chang, J.F., Li, H.Y., Hou, T., Li, F., 2016. Biosens. Bioelectron. 86, 971–977.
Cheng, N., Song, Y., Fu, Q.Q., Du, D., Luo, Y.B., Wang, Y., Xu, W.T., Lin, Y.H., 2018. Biosens. Bioelectron. 117, 75–83.
Cui, H.F., Zhang, T.T., Lv, Q.Y., Song, X., Zhai, X.J., Wang, G.G., 2019. Biosens. Bioelectron. 141, 111452.
Deng, H.H., Li, K.L., Zhuang, Q.Q., Peng, H.P., Zhuang, Q.Q., Liu, A.L., Xia, X.H., Chen, W., 2018. Nanoscale 10, 6467–6473.
Dong, J.X., Gao, Z.F., Zhang, Y., Li, B.L., Li, N.B., Luo, H.Q., 2017. Biosens. Bioelectron. 91, 155–161.
Ge, X., Asiri, A.M., Du, D., Wen, W., Wang, S., Lin, Y., 2014. TrAC Trends Anal. Chem. 58, 31–39.
Hakonen, A., Beves, J.E., 2018. ACS Sens. 3, 2061–2065.
Hao, T., Li, J.J., Yao, F.L., Dong, D.Y., Wang, Y., Yang, B.G., Wang, C.Y., 2017. ACS Nano 11, 5474–5488.
Hsu, M.N., Wei, S.C., Phan, D.T., Zhang, Y., Chen, C.H., 2019. Adv. Healthc. Mater. 8, 1801277.
Hu, T., Xu, J., Ye, Y., Han, Y., Li, X., Wang, Z., Sun, D., Zhou, Y., Ni, Z., 2019. Biosens. Bioelectron. 136, 112–117.
Hu, X., Liu, X.D., Zhang, X.D., Chai, H.X., Huang, Y.M., 2018. Biosens. Bioelectron. 105, 65–70.
Jia, X., Li, J., Wang, E., 2013. Small 9, 3873–3879.
Jin, R., Kong, D., Yan, X., Zhao, X., Li, H., Liu, F., Sun, P., Lin, Y., Lu, G., 2019. ACS Appl. Mater. Interfaces 11, 27605–27614.
Kim, J., Jeerapan, I., Sempionatto, J.R., Barfidokht, A., Mishra, R.K., Campbell, A.S., Hubble, L.J., Wang, J., 2018. Accounts Chem. Res. 51, 2820–2828.
Kong, D.S., Jin, R., Zhao, X., Li, H.X., Yan, X., Liu, F.M., Sun, P., Gao, Y., Liang, X.S., Lin, Y.H., Lu, G.Y., 2019. ACS Appl. Mater. Interfaces 11, 11857–11864.
Lei, C.Y., Dai, H., Fu, Y.C., Ying, Y.B., Li, Y.B., 2016. Anal. Chem. 88, 8542–8547.
Li, J., Mo, L., Lu, C.H., Fu, T., Yang, H.H., Tan, W., 2016. Chem. Soc. Rev. 45, 1410–1431.
Li, J., Mooney, D.J., 2016. Nat. Rev. Mat. 1, 16071.
Liu, M., Khan, A., Wang, Z.F., Liu, Y., Yang, G.J., Deng, Y., He, N.Y., 2019. Biosens. Bioelectron. 130, 174–184.
Long, Q., Li, H.T., Zhang, Y.Y., Yao, S.Z., 2015. Biosens. Bioelectron. 68, 168–174.
Mahato, K., Srivastava, A., Chandra, P., 2017. Biosens. Bioelectron. 96, 246–259.
Masia, A., Suarez-Varela, M.M., Llopis-Gonzalez, A., Pico, Y., 2016. Anal. Chim. Acta 936, 40–61.
Miao, H., Zhong, D., Zhou, Z.N., Yang, X.M., 2015. Nanoscale 7, 19066–19072.
Parrilla Vázquez, P., Ferrer, C., Martínez Bueno, M.J., Fernández-Alba, A.R., 2019. TrAC Trends Anal. Chem. 115, 13–22.
Pundir, C.S., Malik, A., Preety, 2019. Biosens. Bioelectron. 140, 111348.
Qing, Z.H., Zhu, L.X., Yang, S., Cao, Z., He, X.X., Wang, K.M., Yang, R.H., 2016. Biosens. Bioelectron. 78, 471–476.
Quesada-Gonzalez, D., Merkoci, A., 2015. Biosens. Bioelectron. 73, 47–63.
Santopolo, G., Domenech-Sanchez, A., Russell, S.M., de la Rica, R., 2019. ACS Sens. 4, 961–967.
Sun, Z.W., Tian, L.Y., Guo, M., Xu, X.T., Li, Q., Weng, H.B., 2017. Food Control 81, 23–29.
Supraja, P., Tripathy, S., Krishna Vanjari, S.R., Singh, V., Singh, S.G., 2019. Biosens. Bioelectron. 141, 111441.
Tan, L.L., Chen, Z.B., Zhang, C., Wei, X.C., Lou, T.H., Zhao, Y., 2017. Small 13, 1603370.
Tang, W.Z., Yang, J.X., Wang, F., Wang, J.L., Li, Z.H., 2019. Anal. Chim. Acta 1060, 97–102.
Vikrant, K., Tsang, D.C.W., Raza, N., Giri, B.S., Kukkar, D., Kim, K.H., 2018. ACS Appl. Mater. Interfaces 10, 8797–8817.
Wang, X.Z., Hou, T., Dong, S.S., Liu, X.J., Li, F., 2016. Biosens. Bioelectron. 77, 644–649.
Willner, I., 2017. Accounts Chem. Res. 50, 657–658.
Wu, S., Li, D.D., Gao, Z.M., Wang, J.M., 2017. Microchim. Acta 184, 4383–4391.
Wu, Y., Jiao, L., Xu, W.Q., Gu, W.L., Zhu, C.Z., Du, D., Lin, Y.H., 2019. Small 15, 1900632.
Yan, L., Zhu, Z., Zou, Y., Huang, Y., Liu, D., Jia, S., Xu, D., Wu, M., Zhou, Y., Zhou, S., Yang, C.J., 2013. J. Am. Chem. Soc. 135, 3748–3751.
Yan, X., Li, H.X., Hu, T.Y., Su, X.G., 2017a. Biosens. Bioelectron. 91, 232–237.
Yan, X., Li, H.X., Su, X.G., 2018. Trac. Trends Anal. Chem. 103, 1–20.
Yan, X., Song, Y., Wu, X.L., Zhu, C.Z., Su, X.G., Du, D., Lin, Y.H., 2017b. Nanoscale 9, 2317–2323.
Yan, X., Wang, T., Yao, D., Xu, J., Luo, Q., Liu, J., 2019. Small 15, 1900350.
Zhan, Y.J., Zeng, Y.B., Li, L., Luo, F., Qiu, B., Lin, Z.Y., Guo, L.H., 2019. ACS Sens. 4, 1252–1260.
Zhang, J., Mou, L., Jiang, X., 2018. Anal. Chem. 90, 11423–11430.
Zhang, S.X., Xue, S.F., Deng, J.J., Zhang, M., Shi, G.Y., Zhou, T.S., 2016. Biosens. Bioelectron. 85, 457–463.
Zhao, L.H., Yin, S., Ma, Z.F., 2019. ACS Sens. 4, 450–455.
Zhu, Z., Guan, Z., Jia, S., Lei, Z., Lin, S., Zhang, H., Ma, Y., Tian, Z.Q., Yang, C.J., 2014. Angew. Chem. 53, 12503–12507.